Hindawi
Journal of Engineering
Volume 2023, Article ID 1062388, 14 pages
https://doi.org/10.1155/2023/1062388

Research Article

GIS-Based Landslide Susceptibility Mapping Using Frequency Ratio and Shannon Entropy Models in Dejen District, Northwestern Ethiopia

Abinet Addis

Department of Civil Engineering, University of Debre Markos, Debre Markos, Ethiopia

Correspondence should be addressed to Abinet Addis; abinetaddis2002@gmail.com

Received 6 July 2022; Revised 13 December 2022; Accepted 11 January 2023; Published 2 February 2023

Academic Editor: Kartik Ariyur

A GIS-based study has been carried out to map areas landslide susceptibility using both frequency ratio (FR) and Shannon entropy (SE) bivariate statistical models. A total of 270 landslides were identified and classified randomly into training landslides datasets (70%) and the remaining (30%) of landslides datasets were used for validation purpose. The 11 landslides conditioning factors like slope, elevation, aspect, curvature, topographic wetness index, normalized difference vegetation index, distance from road, distance from river, distance from faults, land use, and rainfall were integrated with training landslides to determine the weights of each landslide conditioning factor and factor classes using both frequency ratio and Shannon entropy models. The landslide susceptibility maps were produced by overlay the weights of all the landslide conditioning factors using raster calculator of the spatial analyst tool in ArcGIS 10.4. The final landslide susceptibility maps were reclassified as very low, low, moderate, high, and very high susceptibility classes both FR and SE models. This susceptibility maps were validated using landslide area under the curve (AUC). The results of AUC accuracy models showed that the success rates of the FR and SE models were 0.761 and 0.822, while the prediction rates were 0.753 and 0.826, respectively.

1. Introduction

Landslides are one of the nature hazards causing a lot of casualties and property losses of all over the world [1, 2]. Natural hazards such as landslides, flood, earthquake, and drought risk cannot be avoided completely but the processes and consequences can be mitigated [3, 4]. Landslides are more widespread than any other geological event and can occur anywhere in the world. They occur when large masses of soil, rocks, or debris move down a slope due to the effect of a natural phenomenon or human activity [5, 6].

In Ethiopia, landslides, mostly manifested as rock fall, earth slide, debris, and mudflow are among the major geohazards, especially in the steep and hilly areas of the highlands with greater than 1500 m altitude [7, 8]. According to M. Meten et al. [9], from 1960 to 2010, about 388 people are reported dead, 24 injured and a great deal of agricultural lands, houses, and infrastructures were affected. The occurrence of landslides is an extremely complex phenomenon which depends upon various factors such as geologic structure, lithological association, topography, rainfall, earthquake, and human activity [10]. One of the most widely used approaches to reduce the landslide damages is preparing a landslide susceptibility mapping using suitable models and selecting the effective conditioning factors [11, 12]. Over the last decades, many studies have made contributions in landslide susceptibility maps using qualitative and quantitative methods. Some of the methods include the frequency ratio model [2, 4, 13–18]. A combination of both FR and SE have been applied for landslide susceptibility mapping [19–24], weights of evidence model [12, 25–29], and Shannon entropy model [11, 30–33]. Landslide susceptibility models are based on the bivariate FR and WOE models [34] and frequency ratio and information value models [1, 10, 35]. Landslide susceptibility models based on the bivariate frequency ratio and

multivariate logistic regression models [36–40] etc., are used with the development of the GIS techniques. GIS platforms help in the calculation and visualization of the cumulative effects of conditioning factors on landslides.

In this study, we have used Shannon entropy (SE) and frequency ratio (FR) models for the development of landslide susceptibility maps of Dejen district, Ethiopia. Dejen district, one of the most landslide occurrence districts in northwestern part of Ethiopia with the area of Abay Gorge along the highway main road from Addis Ababa to Bahir Dar. Abay Gorge (Dejen to Goha Tsion) road is reputedly damaged and interrupted by the case of landslide occurrence, especially in the summer season. So, to address all these issues, the results of this study can help for decision makers to delineate the landslide occurrence areas in the study area.

2. Materials and Methods

2.1. Study Area. Dejen district is located in the northwestern part of Ethiopia with an area of 557.48 km^2. According to UTM coordinate system, the location of Wereda is approximately between longitude 395000 m E425000 m E and latitude 1110000 m N–1140000 m N direction as shown in Figure 1. Topographically, the altitude ranges from 991 m to 2559 m and the slope angle varies from 0 to 66 degrees. In terms of land use, most of the Wereda is covered by scrub/shrub and agricultural area. The study area receives high amount of rainfall during the summer season. The average recorded annual precipitation of the area was 1070 mm. The geological units of the study area encompass eight distinct features with the stepwise. The geological age of these formations are Palaeozoic and Mesozoic era that composed of sandstones, limestone, gypsum, and shale [22].

2.2. Data Source and Methodology. In this research, to achieve the main objective was after using primary and secondary data. The primary data were collected from field survey and observation and the secondary data for the study were acquired from governmental institutions, journals, internet, and other documents. The main data used for this study were land sentinel 2 images and ASTER GDEM of the area with spatial resolution of 30 m, Google Earth imagery and topographical map of the area. The data layer of land use and NDVI was derived from sentinel 2 images and ASTER GDEM data used to create the slope, elevation, aspect, curvature, TWI, and river networks data layers and their extents through spatial analysis tools. Another data were used in this study, the average annual rainfall of metrological data and geological map of the study area. The geological map was used to create faults layer of the study area. In the present study, various thematic maps were prepared by digitized from Google Earth imagery, topographical and geological maps of the area. The main road networks were digitized from the topographical map and the fault layer was digitized from geological map. The other data sets of landslides were digitized from the study area of Google Earth imagery, shows in Table 1. All the data layers have been constructed and combined in ArcGIS 10.4 tool. ArcGIS tool was applied throughout the whole process in this study. Accordingly, the FR and SE models were used to generate elaborative landslide susceptibility maps. For the purpose of assessment and validation of landslide susceptibility maps, the AUC methods were used, as shown in Figure 2.

2.3. Landslide Inventory Map. Landslide inventory mapping is the systematic mapping of existing landslides in a region using various techniques such as field survey, aerial photographs or Google Earth imagery interpretation, satellite image interpretation, literature search for historical landslide records, technical and scientific reports, governmental reports, and the interview of experts [41, 42]. In this research, the landslide inventory map which has a total of 280 single landslide locations was created based on Google Earth imagery digitized into points using GIS 10.4 and field visits. Though there is no specific rule for defining how landslide occurrence will be allocated into training and validation data sets [43], usually research work has been done by using 70% of landslides events as training data sets for preparing landslide susceptibility model and the rest 30% have been used for validation of the output model [11, 14, 44]. In this study, 196 (70%) of the landslides were used to training landslide susceptibility models and the remaining 84 (30%) of the landslides were used to model validation, as shown in Figure 3.

2.4. Landslide Conditioning Factors. To identify a landslide occurrence conditioning factors is a very complex task. Because there is no standard rule to select which factor to be used or not, rather than deciding on the nature of area and data availability [45]. In this study, eleven conditioning factors were selected based on the literature, effectiveness, availability of data, and the relevance with respect to land slide occurrence [23]. These conditioning factors are slope, elevation, aspect, and curvature, topographic wetness index, normalized difference vegetation index, distance from road, distance from river, and distance from faults, land use, and rainfall. All the selected conditioning factors were used to perform the landslide susceptibility mapping. Each factor was converted to a raster format with a spatial resolution 30×30 m and was classified based on the Jenks natural breaks method in ArcGIS application, shown in Figure 4.

In landslide susceptibility studies, slope is considered one of the major contributions of landslide conditioning factor of slope failure [21, 46]. According to the importance of the slope conditioning factor in the landslide occurrence, the study area was classified into seven classes in degree. With increase in slope angle, the possibility of landslide occurrence increases [19, 47, 48]. Elevation is an important conditioning factor in landslide susceptibility mapping and it also impacts the environmental conditions on slopes such as human activity, vegetation, soil moisture, and climate [49, 50]. Curvature plays an important role in the surface run off and ground infiltration, thus affecting the erosion of the surface and ground water condition of the region [17]. The curvature map of the study area was classified into concave (negative), convex (positive), and flat (zero) surfaces. In the case of

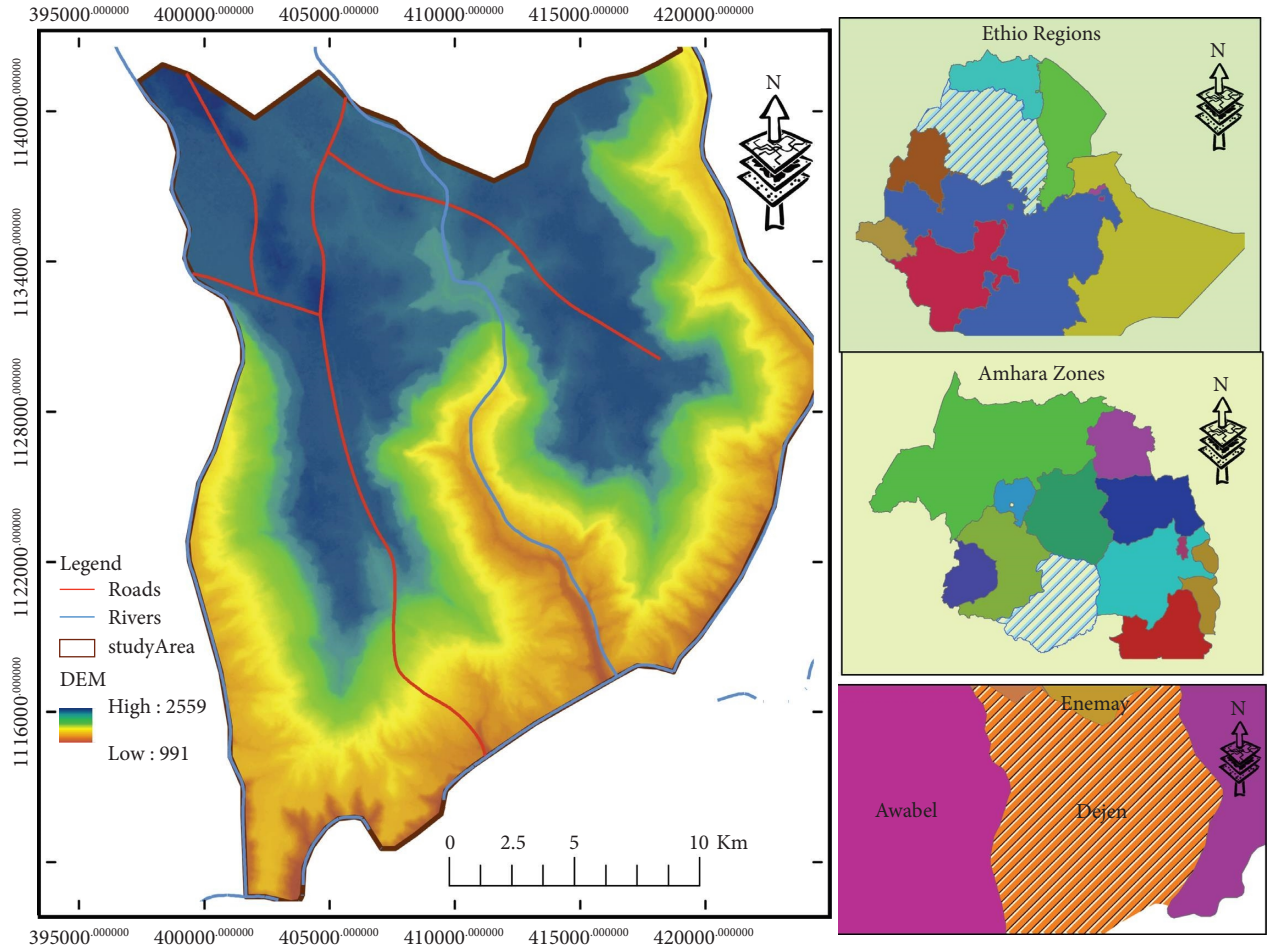

Figure 1: Location map of the study area.

Table 1: Type of conditioning factors, format, and source.

Type conditioning factors	Format	Sources
Slope Elevation Aspect Curvature Topographic witness index (TWI) River	Raster	Derived from of ASTER GDEM image (2021)
Faults	Vector	Digitized from the study area of geological map, Minister of Water and Energy, Addis Ababa, Ethiopia
Road	Vector	Digitized from the study area of topographic map, Minister of Water and Energy, Addis Ababa, Ethiopia
Land use NDVI	Vector Vector	Analysed from Sentinel 2 images in the USGS (2021)
Rainfall	Vector	Interpretation of Ethiopian National Metrological Agency, Addis Ababa (1990–2021)
Landslide inventory	Vector	Digitized from Google Earth imagery (2021) and field survey

curvature, the more negative the value, the higher the probability of landslide occurrence [29]. Aspect represents the direction that a slope faces [49]. Slope aspect affects erosion, surface evaporation, desertification, solar heating, and surface weathering, thus affecting the occurrence of landslides [46, 51]. Topographic wetness index (TWI) is among one of the important factors responsible for the landslide, which can quantitatively display the control of terrain on the spatial

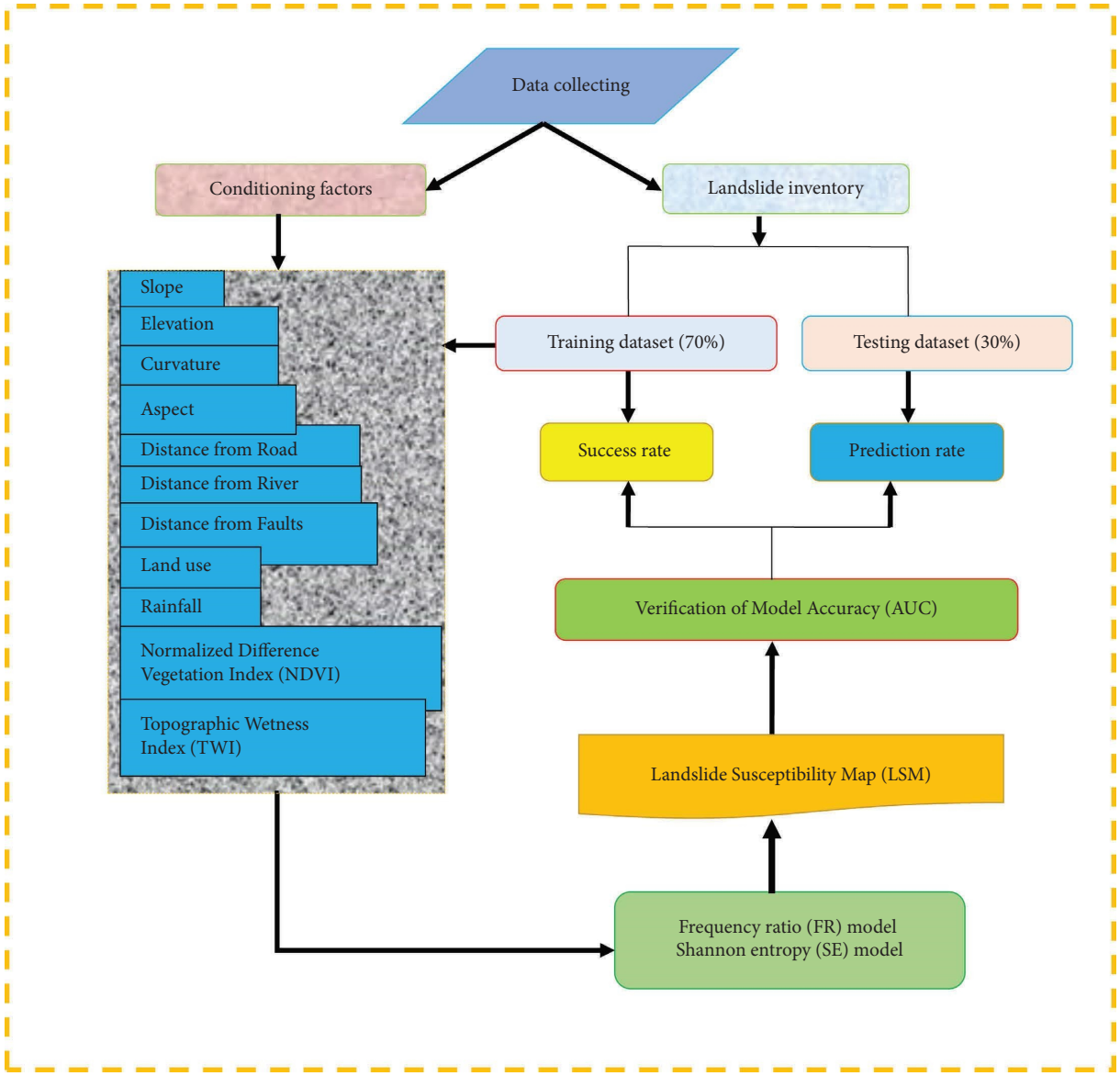

Figure 2: Workflow of the methodology.

distribution of soil moisture, is a widely used terrain attribute. The TWI conditioning factor was obtained from DEM with 30 m spatial resolution by the following equation:

$$\text{TWI} = Ln\left(\frac{A_S}{\tan\beta}\right), \tag{1}$$

where A_s is the specific catchment area (m^2/m) and β is slope angle in degrees [52]. TWI is used to measure the topographic control of hydrological procedures [53]. Rainfall is considered to be one of the landslides occurrences a conditioning factor. Rainfall map was prepared using station locations in the study area through the IDW interpolation method of annual average precipitation (1990–2021). Distance to road is one of the most effective factors on landslide occurrence in a hilly area [1]. Road construction near the hillside may lead to changes in the natural conditions of areas. Distance to river networks plays an important role in landslide occurrence factor closely to surface water. The NDVI conditioning factor was obtained from Sentinel-2 satellite imagery with 30 m spatial resolution by the following equation:

$$\text{NDVI} = \frac{IR - R}{IR + R}, \tag{2}$$

where IR is the infrared and R is the red bands of the electromagnetic spectrum. NDVI values range between −1.0 and 1.0, where any negative values are mainly generated from clouds, water, and snow and values near zero are mainly generated from rock and bare soil and the positive value indicates that the ground is covered by vegetation. Land use is an important conditioning factor that affects the occurrence of landslides. The map of land use was derived from Sentinel-2 satellite imagery, by using a supervised classification technique in ArcGIS. The land use map was classified into six classes. The study area is predominantly covered with the

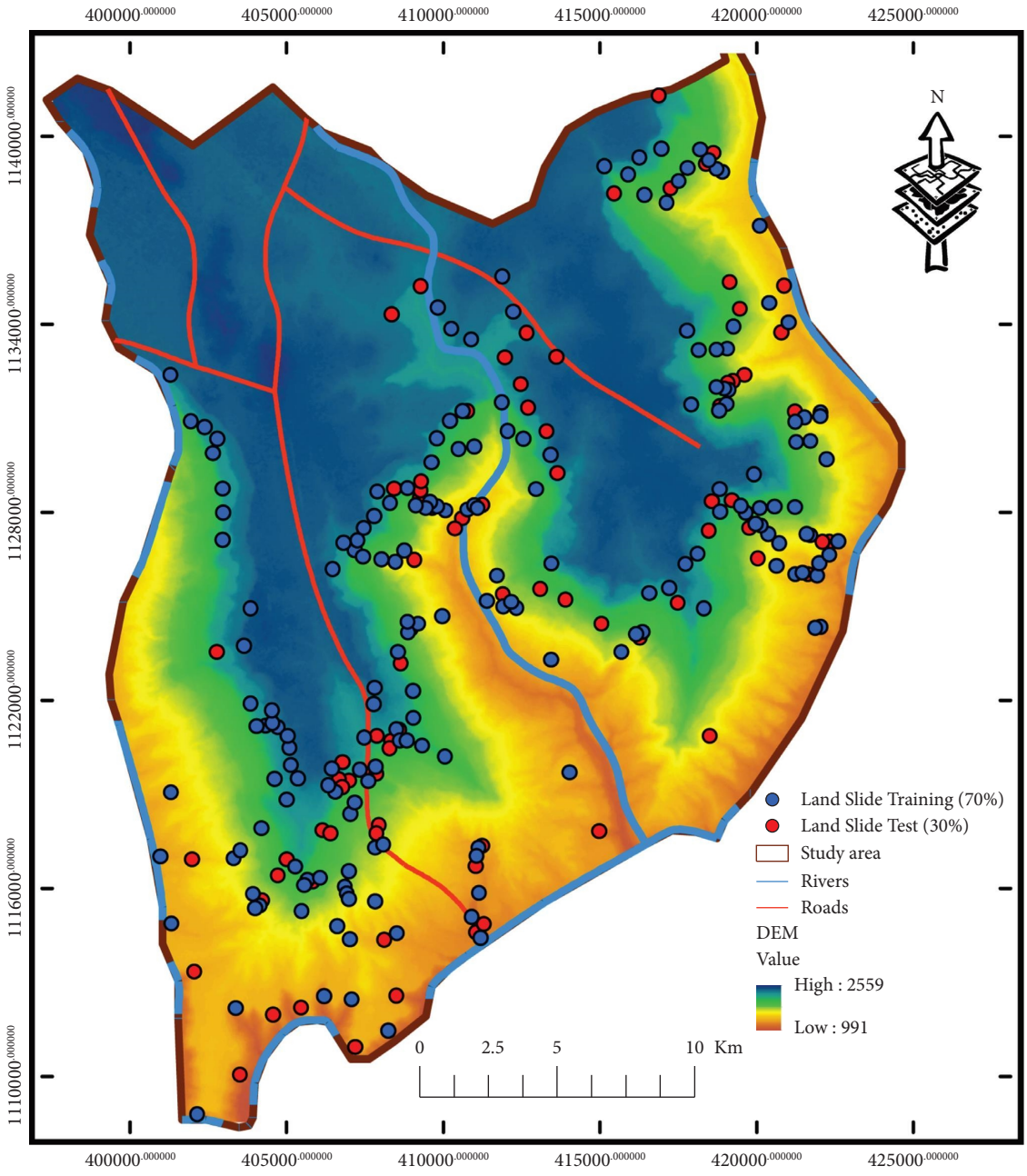

Figure 3: Landslide inventory map.

cropland and scrubs. Distance to faults is considered a highly landslides conditioning factor in many research studies [31, 37, 54, 55]. The strength of rocks decreases with the amount of joints, which increase with the distance to faults [12].

2.5. Landslide Susceptibility Modeling

2.5.1. Frequency Ratio (FR) Model. Frequency ratio is one of the most widely adopted and popular methods for landslide susceptibility assessment [14, 16]. FR is one of the most cited bivariate statistical analysis methods in natural hazard studies, like flood, landslide, and drought hazard [56]. The frequency ratio is the ratio of the area where landslides occurred in the total study area and also is the ratio of the probabilities of a landslide occurrence to a non-landslide occurrence for a given attribute [57, 58]. Generally, a greater ratio indicates a stronger relationship between a conditioning factor and landslide and vice versa. A value of 1 is an average value for the area landslides occurring in the total area. If the FR value is greater than 1, it indicates a high probability of landslide occurrence, and a value less than 1 indicates a low relationship between probabilities of landslide occurrence. The landslides susceptibility map (LSM) can be calculated by summing the FR of all of the factors considered in the following equation:

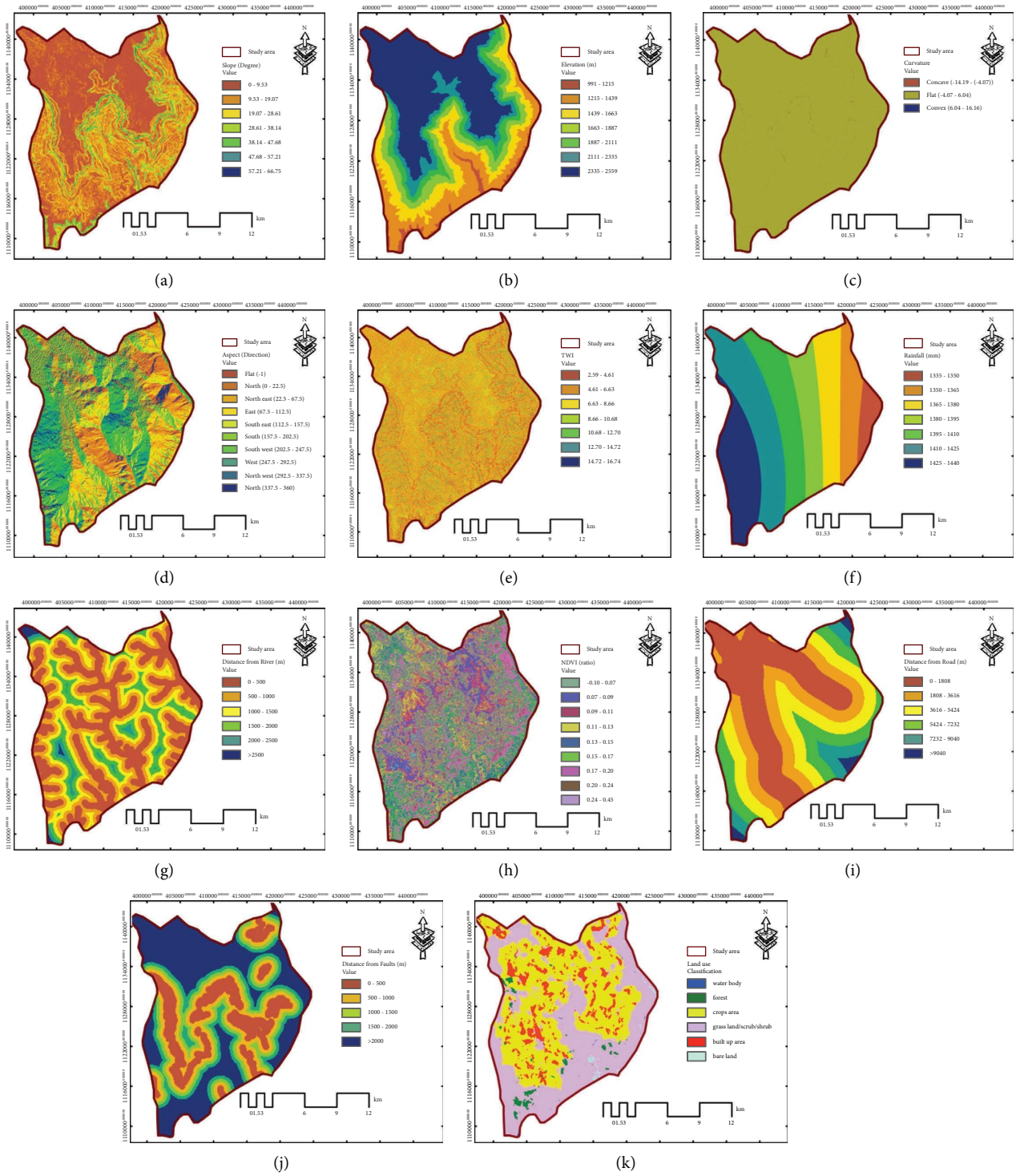

FIGURE 4: Landslide conditioning factors. (a) Slope. (b) Elevation. (c) Curvature. (d) Aspect. (e) Topographic Witness Index (TWI). (f) Rainfall. (g) River networks. (h) NDVI. (i) Road. (j) Faults. (k) Land use.

$$\mathrm{LSM} = \sum_{j=1}^{n} \mathrm{FR}, \tag{3}$$

where LSM is landslide susceptibility map and FR represents for each factor type or class, n is the number of factors. FR was applied and the weights were assigned to each class of each conditioning factor. The FR can be obtained by the following equation as follows:

$$\mathrm{FR} = \left[\frac{N_{\mathrm{pix}}\left(SX_i\right) / \sum_{i=1}^{m} SX_i}{N_{\mathrm{pix}}\left(X_j\right) / \sum_{j=1}^{n} N_{\mathrm{pix}}\left(X_j\right)} \right], \tag{4}$$

where the number of landslide pixels in class i of the factor X is represented by $N_{\text{pix}}(SX_i)$; the total number of pixels within factor X_j is represented by $N_{\text{pix}}(X_j)$; m is the number of classes in factor X_i; and n is the total number of factors in the study area [58].

2.5.2. Shannon Entropy (SE) Model. The second model used for LSM in this study is the bivariate of the Shannon entropy model. The Shannon's entropy model is an improvement on the frequency ratio model [59]. Shannon's entropy measures the instability, disturbance, or uncertainties of a system [20]. In fact, Shannon's entropy states a way to estimate main factors among effective factors of an objective weight of the index system. The following equations were used to calculate the information of the coefficient:

$$E_{ij} = \frac{\text{FR}}{\sum_{j=1}^{sj} \text{FR}},$$

$$H_j = -\sum_{j=1}^{sj} \left(E_{ij}\right) \log_2 \left(E_{ij}\right), H_{j\max} = \log_2 S_j, S_j \text{ is number of class}, I_j = \frac{H_{j\max} - H_j}{H_{j\max}}, \quad I = (0, 1),\ j = 1 \ldots n,\ W_j = I_j * \text{FR}, \tag{5}$$

where FR is frequency ratio, E_{ij} is the probability density for each class I in factor j;H_j and $\text{H}_{j\max}$ are entropy values; I_j is the information coefficient of factor j; S_j is the number of classes; and W_j is the final weight of each factor. The final landslide susceptibility map (LSM) was calculated using the following equation:

$$W_j = I_j * \text{FR}, \tag{6}$$

where i is the number of particular parametric map; **z** is the number of classes within parametric map with the greatest number of classes; m_{i} is the number of classes within particular parametric map; C is value of the class after secondary classification; and w_j is the weight of a parameter.

3. Results and Discussion

3.1. Frequency Ratio (FR) Model. FR was measured for each class of every landslide conditioning factor by dividing the landslide occurrence ratio by the area ratio. The results of the FR model for each of the classes of effective factors are shown in Table 2. In general, the FR value of 1 indicates the average correlation between landslide occurrence and effective factors. If the FR value would be greater than 1, there is a high landslide occurrence and FR value less than 1 indicates that low landslide occurrence [43]. The analysis of FR for the relationship between landslide occurrence and slope degree indicate that class 47.68°–57.21°, the highest FR value of 11.316 among the other classes of slope degree and followed by 57.21°–66.75°, 38.14°–47.68°, 28.61°–38.14°, and 19.07°–28.61°, the FR ratios 9.613, 5.869, 3.924, and 2.027, respectively. Subsequently, at slopes class 0°–9.53° and 9.53°–19.07° (FR = 0.161 and FR = 0.694), respectively, indicating a low probabilities of landslide occurrence. In the study area, was observed that when landslide occurrence probability increased as the slope gradient increased up to a certain extent, and then, it decreased with results of other literature studies [20]. Because the higher slope values trigger the effect of gravity and also increase shear stress [42].

According to the relationship between landslide occurrence and elevation factor indicate that the ranges between 991 m–1215 m and 1215 m–1439 m, (FR = 0.599 and FR = 0.696, respectively), which implies a low probabilities of landslide occurrence in the study area. The elevation ranges between 1439 m–1663 m, 1663 m–1887 m, 1887 m–2111 m, and 2111 m–2559 m and has the highest FR values (1.211, 1.573, 1.872, and 2.746, respectively), indicating a high probabilities of landslide occurrence. In the study area, as the elevation increases, the probability of landslide occurrence increases up to a certain extent, and then, it decreased. In the case of aspect factor classes are the most abundance on east facing (FR = 1.872), south east facing (FR = 2.147), south facing (FR = 1.627), and south west facing (FR = 1.153), indicating a high probabilities of landslide occurrence. However, the remaining aspect classes have the lowest abundance of FR value less than 1, it indicates that a low probabilities of landslide occurrence. Considering the case of land use, results show that the agricultural land, scrub/shrub, and bare land use types have values of FR (1.105, 1.026, and 1.280, respectively), which implies that a high probabilities of landslide occurrence. The highest FR value of agricultural land, scrub/shrub, and bare land is due to its exposure to erosion and soil moisture [37]. In the case of curvature, factor classes of concave (−14.19–(−4.07)) and convex (6.04–16.16) have the highest value of FR (8.840 and 10.026), respectively, indicating a high probabilities of landslide occurrence. Subsequently, curvature class of a flat slope (−4.07–6.04) has a low FR value (0.968), indicating low probabilities of landslide occurrence in this area. The distance from road classes 1808 m–3616 m and 3616 m–5424 m with a value of FR (1.643 and 1.282), respectively, has the greatest impact on landslide coherence. In the study area, the landslide frequency increases as the distance from roads decreases. Therefore, the existing road and the ongoing constructions disturb the stability of slope there by increasing the probability of landslide occurrence with results of other literature studies [19, 20]. According to F. Guzzetti

[60], the landslide probability decreases with the increasing distance from river networks. In this study area, distance from river networks, 0–500 m class exerts the highest influence on landslide occurrence in this study. The reason is that permanent rivers are the main source of moisture for landslide occurrence. According to the results for distance from faults, the class of 0–500 m with a value of FR (2.551) has the greatest impact on landslide occurrence in the study area. In the NDVI, the FR value is greater than one, where the NDVI classes −0.1–0.07, 0.15–0.17, and 0.17–0.20, indicating a high probabilities of landslides occurrence. This class of NDVI means bare land, built up areas, and scrubs. However, the remaining NDVI classes have low FR value less than one; with relatively high vegetation coverage can easily lead to landslide occurrence. The relationship between TWI landslide probabilities showed that 2.59–4.61, 10.68–12.70, and 14.72–16.74 classes have the highest value of FR (3.043, 1.216, and 10.231), respectively, greater than one. With regard to the conditioning factor rainfall, four classes with 1335–1350 mm, 1350–1365 mm, 1410–1425 mm, and 1425–1440 mm have a higher FR value than the other classes and are the most landslide occurrence classes.

3.2. Shannon Entropy (SE) Model. The results of SE for the relationship of the effective factors with the occurrence of landslides are presented in Table 2. The weight of each conditioning factors in the Shannon's entropy model was based on frequency ratio (FR) values. The results showed that curvature, slope and TWI are the most dominant conditioning factors in the landslide susceptibility with SE weights of ($W_j = 1.481$, $W_j = 0.964$ and $W_j = 0.758$), respectively, followed by distance from faults, distance from river, elevation, aspect, and distance from road with SE weights ($W_j = 0.145$, $W_j = 0.135$, $W_j = 0.129$, $W_j = 0.129$, and $W_j = 0.103$), respectively. In this study area, the reaming conditioning factors are less significant in the landslide occurrence. From the result E_{ij}, it is seen that slope degree interval of 47.68°–57.21° is highly probabilities to landslide occurrence, followed by the slope class 57.21°–66.75°. The other classes have low values. In the case of elevation, the altitude ranges between 2111 m and 2335 m and has a highly probability of landslide occurrence among other classes of elevation. According to aspect, south east facing followed by east facing aspects are the most abundant of landslide occurrence in the study area. In the case of land use, bare land followed by agricultural area, indicating a highly probabilities of landslide occurrence, with relatively a lower vegetation coverage. The E_{ij} value for curvature clearly showed that classes convex (6.04–16.16) and concave (−14.19–(−4.07)), with high values of 0.505 and 0.446, respectively. The distance to roads, 1808 m–3616 m class has the highest E_{ij} value (0.344) followed by 5424 m–7232 m (0.268). However, the remaining classes have a low landslides occurrence in the area. In the case of distance to rivers, the range between 0 and 500 m has a high E_{ij} value among other classes, with indicating that a high prone landslide occurrence. Generally, the distance to rivers shows that the E_{ij} value decreases as the distance to river increases. From this, it is clear that the bank erosion is one of the main triggering factors [30]. According to the results for distance from faults, the class of 0–500 m with a value of E_{ij} (0.474) has the greatest impact on landslide occurrence. In the case of the relationship between landslide occurrence and NDVI, the highest E_{ij} value (0.271) was located in the NDVI class of (−0.1–0.07) has the most effect on the occurrence of landslides. In the case of TWI, 14.72–16.74 class has a very highest E_{ij} value (10.231) with other classes of TWI. In rainfall, the highest E_{ij} value (0.261) was located in the rainfall class of 1335–1350 mm. The results based on the Shannon entropy (SE) model approach show that slope, curvature and TWI are the most important factors which explain better the landslide occurrence and distribution in the study area. It should be noted that the landslide contributing factors may vary from place to place by the nature of area and data availability [45].

3.3. Landslide Susceptibility Maps. The map of each conditioning factor is prepared with the help of ArcGIS 10.4, and then, the frequency ratio values were calculated. The calculated FR values for each pixel in the LSM indicate the relative susceptibility to landslide occurrence. The higher pixel values of LSM have the higher landslide susceptibility while the lower pixel values will have lower susceptibility. The landslide susceptibility map was calculated based on the frequency ratio values that have been determined in the training process that can be added in a raster calculator of ArcGIS 10.4, as follows:

$$\text{LSM} = \left(\begin{array}{c} \text{FR slope} + \text{FR elevation} + \text{FR aspect} + \text{FR land use} + \text{FR curvature} + \text{FR distance from road} + \\ \text{FR distance from river} + \text{FR distance from faults} + \text{FR NDVI\_FR TWI} + \text{FR rainfull} \end{array} \right). \quad (7)$$

The LSM values for the frequency ratio model in the study area range from 218.78 to 611.49. These values were classified into five susceptibility classes of very low, low, moderate, high, and very high susceptibility using the geometrical interval method for visual interpretation (Figure 5(a)). From the output of analysis carried out using the ArcGIS 10.4 (Table 3), the very low and low susceptibility zones cover 13.68% and 27.19% of the study area, respectively; whereas, the moderate, high, and very high susceptibility zones cover 30.46%, 20.72%, and 7.94% of the total area, respectively.

The landslide susceptibility map was produced from the Shannon entropy model (Figure 5(b)). The simplest

Table 2: Spatial relationship between each conditioning factor and landslide occurrence using FR and SE models.

Conditioning factors	Classes	Class pixels	%Class pixels	Landslide pixels	%Landslide pixels	FR	SE				
							P_{ij}	H_j	$H_{j\max}$	I_j	W_j
Slope (degree)	0–9.53	292995	45.924	115	7.377	0.161	0.005	2.244	2.807	0.201	0.964
	9.53–19.07	200398	31.411	340	21.809	0.694	0.021				
	19.07–28.61	88419	13.859	438	28.095	2.027	0.060				
	28.61–38.14	38689	6.064	371	23.797	3.924	0.117				
	38.14–47.68	14084	2.208	202	12.957	5.869	0.175				
	47.68–57.21	3110	0.487	86	5.516	11.316	0.337				
	57.21–66.75	298	0.047	7	0.449	9.613	0.286				
Elevation (m)	991–1215	17080	2.677	25.000	1.604	0.599	0.067	2.525	2.807	0.101	0.129
	1215–11439	104637	16.401	178.000	11.418	0.696	0.078				
	1439–1663	91542	14.348	271.000	17.383	1.211	0.135				
	1663–1887	72600	11.379	279.000	17.896	1.573	0.175				
	1887–2111	60986	9.559	279.000	17.896	1.872	0.209				
	2111–2335	55289	8.666	371.000	23.797	2.746	0.306				
	2335–2559	235859	36.969	156.000	10.006	0.271	0.030				
Aspect (direction)	Flat (–1)	43329	6.791	14	0.898	0.132	0.015	2.845	3.322	0.144	0.129
	North (0–22.5)	72892	11.425	39	2.502	0.219	0.024				
	North east (22.5–67.5)	86215	13.513	154	9.878	0.731	0.082				
	East (67.5–112.5)	80684	12.647	369	23.669	1.872	0.209				
	South east (112.5–157.5)	66712	10.457	350	22.450	2.147	0.239				
	South (157.5–202.5)	67903	10.643	270	17.319	1.627	0.181				
	South west (202.5–247.5)	77019	12.072	217	13.919	1.153	0.129				
	West (247.5–292.5)	67670	10.607	97	6.222	0.587	0.065				
	Nort-west (292.5–337.5)	42777	6.705	38	2.437	0.364	0.041				
	North (337.5–360)	32792	5.140	11	0.706	0.137	0.015				
LULC	Water body	569	0.089	1	0.064	0.719	0.135	2.470	2.585	0.045	0.039
	Forest area	10748	1.684	24	1.539	0.914	0.172				
	Agricultural area	290487	45.523	784	50.289	1.105	0.208				
	Scrub/shrub	282013	44.195	707	45.350	1.026	0.193				
	Built up area	51411	8.057	34	2.181	0.271	0.051				
	Bare land	2879	0.451	9	0.577	1.280	0.241				
Curvature	Concave (–14.19–(–4.07)	2037	0.319	44	2.822	8.840	0.446	1.230	1.585	0.224	1.481
	Flat (–4.07) –(6.04)	635507	99.610	1504	96.472	0.968	0.049				
	Convex (6.04–16.16)	449	0.070	11	0.706	10.026	0.505				
NDVI (ratio)	(–0.1)–0.07	8655	1.357	58	3.720	2.742	0.271	2.972	3.170	0.063	0.070
	0.07–0.09	61467	9.634	112	7.184	0.746	0.074				
	0.09–0.11	100884	15.813	186	11.931	0.755	0.074				
	0.11–0.13	130483	20.452	243	15.587	0.762	0.075				
	0.13–0.15	125227	19.628	299	19.179	0.977	0.096				
	0.15–0.17	109386	17.145	349	22.386	1.306	0.129				
	0.17–0.20	67951	10.651	240	15.394	1.445	0.143				
	0.20–0.24	27246	4.271	65	4.169	0.976	0.096				
	0.24–0.45	6694	1.049	7	0.449	0.428	0.042				
Distance from road (m)	0–1808.02	217352	34.068	365	23.412	0.687	0.144	2.252	2.585	0.129	0.103
	1808.02–3616.04	145198	22.759	583	37.396	1.643	0.344				
	3616.04–5424.06	132792	20.814	416	26.684	1.282	0.268				
	5424.06–7232.08	90241	14.145	161	10.327	0.730	0.153				
	7232.08–9040.10	39954	6.262	30	1.924	0.307	0.064				
	9040.10–10848.12	12456	1.952	4	0.257	0.131	0.027				

Table 2: Continued.

Conditioning factors	Classes	Class pixels	%Class pixels	Landslide pixels	%Landslide pixels	FR	SE				
							P_{ij}	H_j	H_{jmax}	I_j	W_j
Distance from river (m)	0–500	224027	35.114	707	45.350	1.291	0.203	2.256	2.585	0.127	0.135
	500–1000	186094	29.169	405	25.978	0.891	0.140				
	1000–1500	135052	21.168	236	15.138	0.715	0.112				
	1500–2000	69937	10.962	98	6.286	0.573	0.090				
	2000–2500	17047	2.672	109	6.992	2.617	0.411				
	>2500	5836	0.915	4	0.257	0.280	0.044				
Distance from faults (m)	0–500	131605	20.590	819	52.534	2.551	0.474	2.010	2.322	0.134	0.145
	500–1000	94857	14.841	195	12.508	0.843	0.157				
	1000–1500	90898	14.221	177	11.353	0.798	0.148				
	1500–2000	81261	12.713	168	10.776	0.848	0.158				
	>2000	240550	37.635	200	12.829	0.341	0.063				
TWI	2.59–4.61	46390	7.271	345	22.130	3.043	0.172	1.966	2.807	0.300	0.758
	4.61–6.63	367920	57.668	804	51.572	0.894	0.051				
	6.63–8.66	156410	24.516	242	15.523	0.633	0.036				
	8.66–10.68	52382	8.210	125	8.018	0.977	0.055				
	10.68–12.70	13129	2.058	39	2.502	1.216	0.069				
	12.70–14.72	1722	0.270	3	0.192	0.713	0.040				
	14.72–16.74	40	0.006	1	0.064	10.231	0.578				
Rainfall (mm)	1335.13–1350.19	27659	4.335	135	8.659	1.997	0.261	2.682	2.807	0.045	0.049
	1350.19–1365.25	69387	10.876	232	14.881	1.368	0.179				
	1365.25–1380.31	84450	13.237	156	10.006	0.756	0.099				
	1380.31–1395.37	78482	12.301	81	5.196	0.422	0.055				
	1395.37–1410.43	108772	17.049	264	16.934	0.993	0.130				
	1410.43–1425.48	155896	24.435	390	25.016	1.024	0.134				
	1425.48–1440.54	113347	17.766	301	19.307	1.087	0.142				

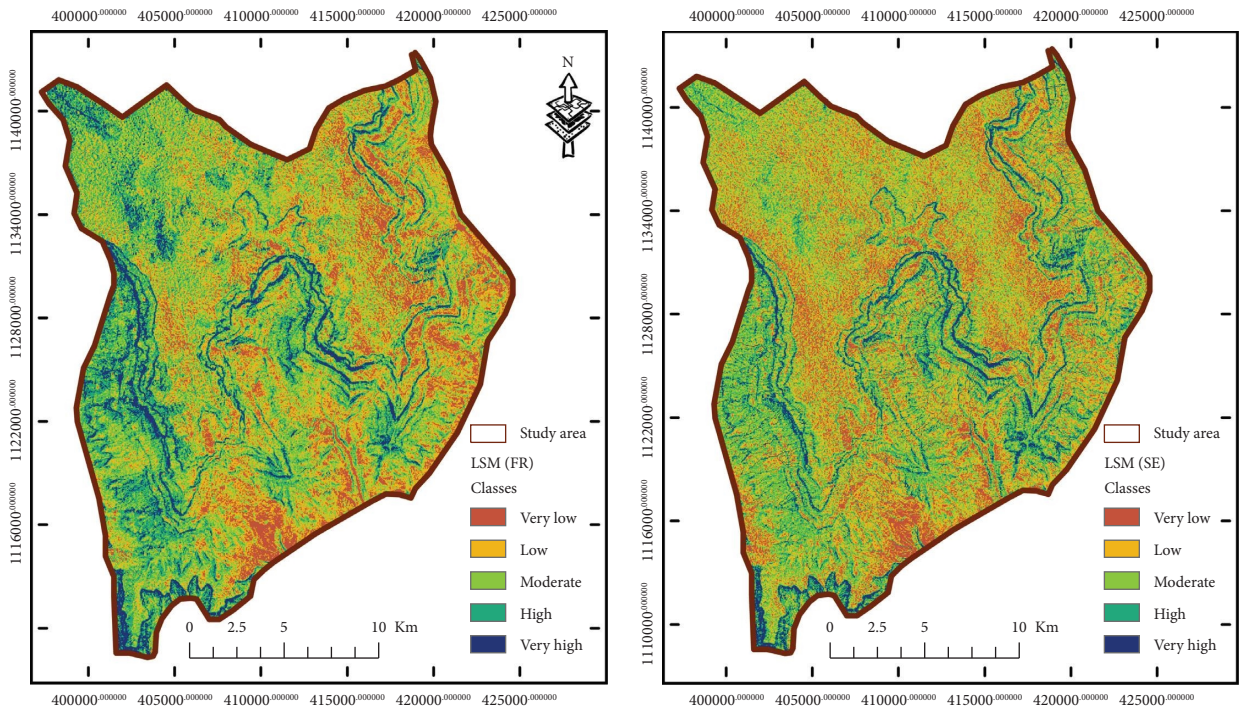

(a) (b)

Figure 5: Landslide susceptibility map using (a) frequency ratio (FR) and (b) Shannon entropy (SE) models.

Table 3: Landslide susceptibility classes and summery of the FR and SE models.

Landslide susceptible classes	*FR model*			*SE model*		
	Range	Area in (km^2)	Area in (%)	Range	Area in (km^2)	Area in (%)
Very low	218.78–330.76	77.39	13.68	6.33–8.04	94.86	16.77
Low	330.76–367.58	153.78	27.19	8.04–9.29	176.47	31.20
Moderate	367.58–404.39	172.25	30.46	9.29–11.00	163.11	28.84
High	404.39–445.81	117.20	20.72	11.00–13.34	97.18	17.18
Very high	445.81–611.49	44.94	7.94	13.34–16.55	33.95	6.00

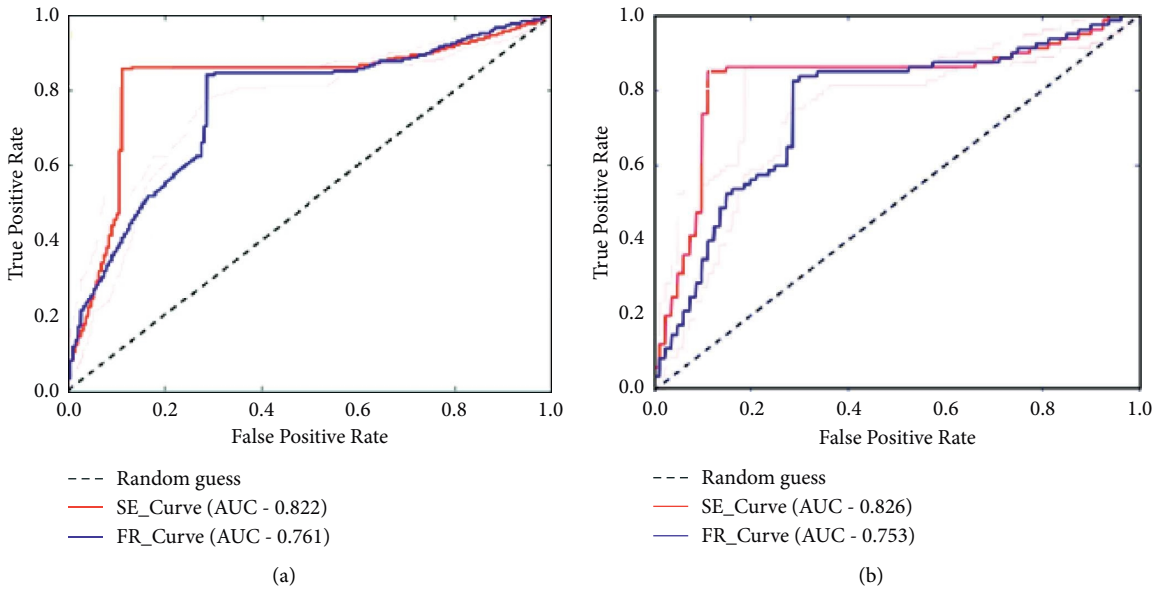

Figure 6: The AUC of success rate curve (a) and predication rate curve (b) of both FR and SE models.

landslide susceptibility equation for this model is given as follows:

$$\begin{aligned}\text{LSM} = {} & (\text{slope} \times 0.964) + (\text{Elevation} \times 0.129) + (\text{Aspect} \times 0.129) + (\text{Land use} \times 0.039) + (\text{Curvature} \times 1.481) \\ & + (\text{Distance from road} \times 0.103) + (\text{Distance from river} \times 0.135) \\ & + (\text{Distance from faults} \times 0.145) + (\text{NDVI} \times 0.070) + (\text{TWI} \times 0.758) + (\text{Rainfall} \times 0.049).\end{aligned} \tag{12}$$

The LSM value varies from 6.33 to 16.55 for the Shannon entropy model. These values were classified into five susceptibility classes of very low, low, moderate, high, and very high susceptibility using the geometrical interval method. Then, the very low susceptible zone covers 16.77% of the total study area, whereas low, moderate, high, and very high susceptible zones cover 31.20%, 28.84%, 17.18%, and 6.00% of the total area, respectively (Table 3).

3.4. Validation of Landslide Susceptibility Maps. After obtaining the landslide susceptibility maps using FR and SE models, their validation is necessary in order to check their reliability. Without model validation, landslide susceptibility maps will not be meaningful. In the present study, the performance of the LSM produced by FR and SE models, were evaluated using area under the curve (AUC). The area under the curve (AUC) is the measure that indicates the accuracy of the landslide susceptibility maps by creating success and prediction rate curves. The success rate curve represented the model fitness to existing landslide and the comparison of the training dataset with the landslide susceptibility map provides the success rate curve. The prediction rate curve indicates the model efficiency to predict future landslide and the comparison of the validation dataset with the landslide susceptibility map provides the prediction rate curve [43, 61]. For this study, 196 (70%) of the landslides were used to training landslide susceptibility models and the remaining 84 (30%) of the landslides were used to model validation. The

success and predictive rate curves can be created for both FR and SE models by using ROC module in ArcGIS 10.4 tool. The AUC rate curves were drawn through the x-axis both the training and validation landslides (true positive rate) and y-axis (false positive rate). The total AUC can be used to determine prediction accuracy of the susceptibility map qualitatively in which larger area means higher accuracy achieved. The AUC value ranges from 0.5 to 1.0 are used to evaluate the accuracy of the model [61]. The qualitative relationship between AUC and prediction accuracy can be classified as follows; excellent (0.9-1.0); very good (0.8-0.9); good (0.7-0.8); average (0.6-0.7), and fair (0.5-0.6), [61]. If AUC value is close to 1.0, then, the model will have ideal performance, where as a value is equal or less than 0.5, then, the model will have poor performance [62]. The result showed that, the AUC of the success rate curves was 0.761 for the FR model and 0.822 for the SE model, which be equivalent to 76.1% and 82.2% predication accuracy, respectively (Figure 6(a)). The AUC of the prediction rate curves were 0.753 for the FR model and 0.826 for the SE model, which be equivalent to 75.3% and 82.6% predication accuracy, respectively (Figure 6(b)). The AUC of the success rate and predictive rate curves range between 0.7 and 0.8, indicating that a good performance of FR model. Also, the success rate and predictive rate curves range between 0.8 and 0.9, indicating a very good performance of the SE model. Therefore, based on the calculated AUC, it is clear that the SE model exhibited better result for landslide susceptibility mapping in the study area.

4. Conclusion

In this study, two bivariate models (i.e., frequency ratio and Shannon entropy models) were used to identify the landslides susceptible areas in Degen Wereda, north western, Ethiopia; using GIS environment has been presented. Eleven landslide conditioning factors were selected based on the availability and effective data. These factors were slope, elevation, aspect, land use, curvature, and distance from road, distance from river networks, and distance from faults, NDVI, TWI, and rainfall to prepare landslide susceptibility maps. A land slide inventory map was prepared using Google Earth imagery and filed survey assessment. For this process, 280 landslide locations were identified and mapped. Also classified into 70% (196) landslides were used to training and 30% (84) of the landslides were used to validation purpose. The susceptibility maps produced by FR and SE models were divided into five susceptibility classes such as very low, low, moderate, high, and very high susceptibility classes based on the geometric interval method. The AUC rate curve quantitatively indicates the performance of the susceptibility maps. The model of Shannon entropy results showed that the accuracies of success rate (82.20%) and predicative rate (82.60%) of the landslide susceptibility map. Similarly, the model of frequency ratio results showed that the accuracies of success rate (76.10%) and predicative rate (75.30%) of the landslide susceptibility map. So, the Shannon entropy (SE) model has a higher AUC than the frequency ratio (FR) model. Finally, this study confirmed that the models of FR and SE were found to be simple, reliable, and effective models for landslide susceptibility mapping of the study area. The final output of landslide susceptibility maps can help the decision makers as basic information for the concerned authorities of government and non-government, district and zonal level of land use planning to perform proper actions in order to prevent and mitigate the existing and future landslides occurrence.

Data Availability

The data used to support the findings of this study are available from the corresponding author upon request.

Conflicts of Interest

The authors declare that they have no conflicts of interest.

Acknowledgments

The authors convey their thanks to authors and staff of Civil Engineering Department, University of Debre Markos, Ethiopia. This research was funded by the authors.

References

[1] B. Li, N. Wang, and J. Chen, "GIS-based landslide susceptibility mapping using information, frequency ratio, and artificial neural network methods in qinghai province, northwestern China," *Advances in Civil Engineering*, vol. 2021, Article ID 4758062, 14 pages, 2021.

[2] S. C. Pal and I. Chowdhuri, "GIS-based spatial prediction of landslide susceptibility using frequency ratio model of Lachung River basin, North Sikkim, India," *SN Applied Sciences*, vol. 1, no. 5, pp. 416–425, 2019.

[3] P. Gyawali, Y. M. Aryal, A. Tiwari, K. C. Prajwol, and K. Ansari, "Landslide susceptibility assessment using bivariate statistical methods: a case study of gulmi district," *Western Nepal*, vol. 16, pp. 29–40, 2019.

[4] T. H. Mezughi, J. M. Akhir, A. G. Rafek, and I. Abdullah, "Landslide susceptibility assessment using frequency ratio model applied to an area along the E-W highway (Gerik-Jeli)," *American Journal of Environmental Sciences*, vol. 7, no. 1, pp. 43–50, 2011.

[5] D. M. Cruden, "A simple definition of a landslide," *Bulletin of the International Association of Engineering Geology*, vol. 43, no. 1, pp. 27–29, 1991.

[6] L. Shano, T. K. Raghuvanshi, and M. Meten, "Landslide susceptibility mapping using frequency ratio model: the case of Gamo highland, South Ethiopia," *Arabian Journal of Geosciences*, vol. 14, no. 7, 623 pages, 2021.

[7] G. Mewa and F. Mengistu, "Assessment of landslide risk in Ethiopia: distributions, causes, and impacts," *Landslides*, vol. 10, 2022.

[8] C. Tesfa and K. Woldearegay, "Characteristics and susceptibility zonation of landslides in Wabe Shebelle Gorge, south eastern Ethiopia," *Journal of African Earth Sciences*, vol. 182, Article ID 104275, 2021.

[9] M. Meten, N. PrakashBhandary, and R. Yatabe, "Effect of landslide factor combinations on the prediction accuracy of landslide susceptibility maps in the blue nile gorge of Central

Ethiopia," *Geoenvironmental Disasters*, vol. 2, no. 1, 9 pages, 2015.

[10] S. P. Mandal, A. Chakrabarty, and P. Maity, "Comparative evaluation of information value and frequency ratio in landslide susceptibility analysis along national highways of Sikkim Himalaya," *Spat. Inf. Res.*vol. 26, no. 2, pp. 127–141, 2018.

[11] N. D. Dam, M. Amiri, N. Al-Ansari et al., "Evaluation of shannon entropy and weights of evidence models in landslide susceptibility mapping for the pithoragarh district of uttarakhand state, India," *Advances in Civil Engineering*, vol. 2022, pp. 1–16, Article ID 6645007, 2022.

[12] Z. Anis, G. Wissem, V. Vali, H. Smida, and G. Mohamed Essghaier, "GIS-based landslide susceptibility mapping using bivariate statistical methods in North-western Tunisia," *Open Geosciences*, vol. 11, no. 1, pp. 708–726, 2019.

[13] D. Thapa and B. P. Bhandari, "GIS-based frequency ratio method for identification of potential landslide susceptible area in the siwalik zone of chatara-barahakshetra section, Nepal," *Open Journal of Geology*, vol. 9, no. 12, pp. 873–896, 2019.

[14] Y. X. Zhang, H. X. Lan, L. P. Li, Y. M. Wu, J. H. Chen, and N. M. Tian, "Optimizing the frequency ratio method for landslide susceptibility assessment: a case study of the Caiyuan Basin in the southeast mountainous area of China," *Journal of Mountain Science*, vol. 17, no. 2, pp. 340–357, 2020.

[15] T. D. Acharya, I. T. Yang, and D. H. Lee, "GIS-based landslide susceptibility mapping of Bhotang, Nepal using frequency ratio and statistical index methods," *J. Korean Soc. Surv. Geod. Photogramm. Cartogr.*vol. 35, no. 5, pp. 357–364, 2017.

[16] L. Li, H. Lan, C. Guo, Y. Zhang, Q. Li, and Y. Wu, "A modified frequency ratio method for landslide susceptibility assessment," *Landslides*, vol. 14, no. 2, pp. 727–741, 2017.

[17] H. J. Oh, S. Lee, and S. M. Hong, "Landslide susceptibility assessment using frequency ratio technique with iterative random sampling," *Journal of Sensors*, vol. 2017, pp. 1–21, Article ID 3730913, 2017.

[18] F. E. S. Silalahi, Y. Arifianti, and F. Hidayat, "Landslide susceptibility assessment using frequency ratio model in Bogor, West Java, Indonesia," *Geosci. Lett.*vol. 6, no. 1, 10 pages, 2019.

[19] S. Panchal and A. K. Shrivastava, "A comparative study of frequency ratio, shannon's entropy and analytic hierarchy process (Ahp) models for landslide susceptibility assessment," *ISPRS International Journal of Geo-Information*, vol. 10, no. 9, p. 603, 2021.

[20] A. Jaafari, A. Najafi, H. R. Pourghasemi, J. Rezaeian, and A. Sattarian, "GIS-based frequency ratio and index of entropy models for landslide susceptibility assessment in the Caspian forest, northern Iran," *International journal of Environmental Science and Technology*, vol. 11, no. 4, pp. 909–926, 2014.

[21] L. J. Wang, M. Guo, K. Sawada, J. Lin, and J. Zhang, "A comparative study of landslide susceptibility maps using logistic regression, frequency ratio, decision tree, weights of evidence and artificial neural network," *Geoscience Journal*, vol. 20, no. 1, pp. 117–136, 2016.

[22] T. Melese, T. Belay, and A. Andemo, "Application of analytical hierarchal process, frequency ratio, and Shannon entropy approaches for landslide susceptibility mapping using geospatial technology: the case of Dejen district, Ethiopia," *Arabian Journal of Geosciences*, vol. 15, no. 5, 424 pages, 2022.

[23] A. Es-smairi, "Spatial Prediction of Landslide Susceptibility Using Frequency Ration (FR) and Shannon Entropy (SE) Models," *A Case Study from Northern Rif*, Morocco, 2022.

[24] L. P. Sharma, N. Patel, M. K. Ghose, and P. Debnath, "Development and application of Shannon's entropy integrated information value model for landslide susceptibility assessment and zonation in Sikkim Himalayas in India," *Natural Hazards*, vol. 75, no. 2, pp. 1555–1576, 2015.

[25] N. Getachew and M. Meten, "Weights of evidence modeling for landslide susceptibility mapping of Kabi-Gebro locality, Gundomeskel area, Central Ethiopia," *Geoenvironmental Disasters*, vol. 8, no. 1, p. 6, 2021.

[26] B. Pradhan, H. J. Oh, and M. Buchroithner, "Weights-of-evidence model applied to landslide susceptibility mapping in a tropical hilly area," *Geomatics, Natural Hazards and Risk*, vol. 1, no. 3, pp. 199–223, 2010.

[27] M. Rezaei Mog, M. Khayyam, M. Ahmadi, and M. Farajzadeh, "Mapping susceptibility landslide by using the weight-of-evidence model: a case study in Merek Valley, Iran," *Journal of Applied Sciences*, vol. 7, no. 22, pp. 3342–3355, 2007.

[28] Y. Cao, X. Wei, W. Fan, Y. Nan, W. Xiong, and S. Zhang, "Landslide susceptibility assessment using the Weight of Evidence method: a case study in Xunyang area, China," *PLoS One*, vol. 16, no. 1, pp. 02456688–e245718, 2021.

[29] S. Lee and J. Choi, "Landslide susceptibility mapping using GIS and the weight-of-evidence model," *International Journal of Geographical Information Science*, vol. 18, no. 8, pp. 789–814, 2004.

[30] Q. Wang, W. Li, W. Chen, and H. Bai, "GIS-based assessment of landslide susceptibility using certainty factor and index of entropy models for the Qianyang county of Baoji city, China," *Journal of Earth System Science*, vol. 124, no. 7, pp. 1399–1415, 2015.

[31] A. Kerekes, S. L. Poszet, and A. Gál, "Landslide susceptibility assessment using the maximum entropy model in a sector of the Cluj–Napoca Municipality, Romania," *Revista de Geomorfologie*, vol. 20, no. 1, pp. 130–146, 2018.

[32] M. Shadman Roodposhti, J. Aryal, H. Shahabi, and T. Safarrad, "Fuzzy Shannon entropy: a hybrid GIS-based landslide susceptibility mapping method," *Entropy*, vol. 18, pp. 343–410, 2016.

[33] A. Kornejady, M. Ownegh, and A. Bahremand, "Landslide susceptibility assessment using maximum entropy model with two different data sampling methods," *Catena*, vol. 152, pp. 144–162, 2017.

[34] T. Mersha and M. Meten, "GIS-based landslide susceptibility mapping and assessment using bivariate statistical methods in Simada area, northwestern Ethiopia," *Geoenvironmental Disasters*, vol. 7, no. 1, 20 pages, 2020.

[35] A. Genene, *Landslide Susceptibility Mapping Using GIS-Based Information Value and Frequency Ratio Methods in Gindeberet Area*, Oromia Region, West Shewa Zone, 2021.

[36] T. C. Korma, "GIS-based landslide susceptibility zonation mapping using frequency ratio and logistics regression models in the Dessie area," vol. 12, pp. 1–25, South Wello, 2022.

[37] K. Solaimani, S. Z. Mousavi, and A. Kavian, "Landslide susceptibility mapping based on frequency ratio and logistic regression models," *Arabian Journal of Geosciences*, vol. 6, no. 7, pp. 2557–2569, 2013.

[38] S. Hidayat, H. Pachri, and I. Alimuddin, "Analysis of landslide susceptibility zone using frequency ratio and logistic regression method in hambalang, citeureup district, bogor regency, west java province," *IOP Conference Series: Earth and Environmental Science*, vol. 280, no. 1, Article ID 012005, 2019.

[39] S. Lee and B. Pradhan, "Landslide hazard mapping at Selangor, Malaysia using frequency ratio and logistic regression models," *Landslides*, vol. 4, no. 1, pp. 33–41, 2007.

[40] G. Das and K. Lepcha, "Application of logistic regression (LR) and frequency ratio (FR) models for landslide susceptibility mapping in Relli Khola river basin of Darjeeling Himalaya, India," *SN Applied Sciences*, vol. 1, no. 11, pp. 1453–1522, 2019.

[41] C. Sivakami and Dr. R. Rajkumar, "Landslide vulnerability zone by weights of evidence model using remote sensing and GIS, in kodaikanal taluk (Tamil nadu, India)," *International Journal of Engineering Research*, vol. V9, no. 2, pp. 788–793, 2020.

[42] A. Wubalem, "Modeling of landslide susceptibility in a part of Abay basin, northwestern Ethiopia," *Open Geosciences*, vol. 12, no. 1, pp. 1440–1467, 2020.

[43] B. Pradhan, S. Lee, and M. F. Buchroithner, "Remote sensing and GIS-based landslide susceptibility analysis and its cross-validation in three test areas using a frequency ratio model," *Photogrammetrie, Fernerkundung, GeoInformation*, vol. 2010, no. 1, pp. 17–32, Article ID 0037, 2010.

[44] A. Wubalem, "Landslide susceptibility mapping using statistical methods in Uatzau catchment area, northwestern Ethiopia," *Geoenvironmental Disasters*, vol. 8, no. 1, pp. 1–21, 2021.

[45] L. Ayalew and H. Yamagishi, "The application of GIS-based logistic regression for landslide susceptibility mapping in the Kakuda-Yahiko Mountains, Central Japan," *Geomorphology*, vol. 65, no. 1–2, pp. 15–31, 2005.

[46] G. l. Du, Y. s. Zhang, J. Iqbal, Z. h. Yang, and X. Yao, "Landslide susceptibility mapping using an integrated model of information value method and logistic regression in the Bailongjiang watershed, Gansu Province, China," *Journal of Mountain Science*, vol. 14, no. 2, pp. 249–268, 2017.

[47] B. T. Pham, D. T. Bui, M. Dholakia et al., "A novel ensemble classifier of rotation forest and Naïve Bayer for landslide susceptibility assessment at the Luc Yen district, Yen Bai Province (Viet Nam) using GIS," *Geomatics, Natural Hazards and Risk*, vol. 8, no. 2, pp. 649–671, 2017.

[48] C. Xu, F. Dai, X. Xu, and Y. H. Lee, "GIS-based support vector machine modeling of earthquake-triggered landslide susceptibility in the Jianjiang River watershed, China," *Geomorphology*, vol. 145–146, pp. 70–80, 2012.

[49] H. Shu, Z. Guo, S. Qi, D. Song, H. R. Pourghasemi, and J. Ma, "Integrating landslide typology with weighted frequency ratio model for landslide susceptibility mapping: a case study from lanzhou city of northwestern China," *Remote Sensing*, vol. 13, no. 18, p. 3623, 2021.

[50] S. He, P. Pan, L. Dai, H. Wang, and J. Liu, "Application of kernel-based Fisher discriminant analysis to map landslide susceptibility in the Qinggan River delta, Three Gorges, China," *Geomorphology*, vol. 171–172, pp. 30–41, 2012.

[51] H. Khan, M. Shafique, M. A. Khan, M. A. Bacha, S. U. Shah, and C. Calligaris, "Landslide susceptibility assessment using Frequency Ratio, a case study of northern Pakistan," *The Egyptian Journal of Remote Sensing and Space Science*, vol. 22, no. 1, pp. 11–24, 2019.

[52] N. R. Regmi, J. R. Giardino, and J. D. Vitek, "Modeling susceptibility to landslides using the weight of evidence approach: western Colorado, USA," *Geomorphology*, vol. 115, no. 1–2, pp. 172–187, 2010.

[53] C. Y. Chen and F. C. Yu, "Morphometric analysis of debris flows and their source areas using GIS," *Geomorphology*, vol. 129, no. 3–4, pp. 387–397, 2011.

[54] S. Karim, S. Jalileddin, and M. T. Ali, "Zoning landslide by use of frequency ratio method (case study: deylaman region)," vol. 9, no. 5, pp. 578–583, 2011.

[55] B. Pradhan, S. Mohsen Mousavi, A. Golkarian, S. Amir Naghibi, and B. Kalantar, "GIS-Based groundwater spring potential mapping using data mining boosted regression tree and probabilistic frequency ratio models in Iran," *AIMS Geosciences*, vol. 3, no. 1, pp. 91–115, 2017.

[56] D. Sarkar, S. Saha, and P. Mondal, "GIS-based frequency ratio and Shannon's entropy techniques for flood vulnerability assessment in Patna district, Central Bihar, India," *International journal of Environmental Science and Technology*, vol. 19, no. 9, pp. 8911–8932, 2021.

[57] S. Lee and J. A. Talib, "Probabilistic landslide susceptibility and factor effect analysis," *Environmental Geology*, vol. 47, no. 7, pp. 982–990, 2005.

[58] A. D. Regmi, K. Yoshida, H. R. Pourghasemi, M. R. DhitaL, and B. Pradhan, "Landslide susceptibility mapping along Bhalubang — shiwapur area of mid-Western Nepal using frequency ratio and conditional probability models," *Journal of Mountain Science*, vol. 11, no. 5, pp. 1266–1285, 2014.

[59] A. Haghizadeh, S. Siahkamari, A. H. Haghiabi, and O. Rahmati, "Forecasting flood-prone areas using Shannon's entropy model," *Journal of Earth System Science*, vol. 126, no. 3, 39 pages, 2017.

[60] F. Guzzetti, "Landslide hazard assessment and risk evaluation: limits and prospectives," in *Proceedings of the 4th EGS Plinius Conferences*, Beijing China, October 2002.

[61] E. Yesilnacar and T. Topal, "Landslide susceptibility mapping: a comparison of logistic regression and neural networks methods in a medium scale study, Hendek region (Turkey)," *Engineering Geology*, vol. 79, no. 3–4, pp. 251–266, 2005.

[62] T. Fawcett, "An introduction to ROC analysis," *Pattern Recognition Letters*, vol. 27, no. 8, pp. 861–874, 2006.